Thermodynamics and Premelting Conformational Changes of Phased $(dA)_5$ Tracts†

Shirley S. Chan* and Kenneth J. Breslauer

Department of Chemistry, Rutgers University, Piscataway, New Jersey 08855-0939

Robert H. Austin

Department of Physics, Princeton University, Princeton, New Jersey 08544

Michael E. Hogan

Center for Biotechnology, Baylor College of Medicine, Woodlands, Texas 77381

Received April 30, 1993; Revised Manuscript Received August 26, 1993®

ABSTRACT: Using synthetic 45 bp long DNAs of known sequences, we have studied (i) the unusual structure that the phased A-tracts have at temperatures below 37 °C, (ii) the thermodynamics of the loss of that aberrant structure well below the duplex melting temperature, and (iii) the conformational changes that occur with temperature. Using temperature-dependent circular dichroism, we detect a low-temperature structural transition in a 45-mer duplex with four segments of phased $(dA)_5$ tracks separated by five segments of five randomized G·C pairs, but none in the corresponding isomeric random sequence 45-mer duplex. Differential scanning calorimetry measurements reveal the enthalpy of this preglobal melting transition to be 3.5 kcal/mol·AT pair or 4.4 kcal/mol·AA step. The integrated enthalpy change for this helix-to-helix intramolecular event only is about 16% of the global duplex-to-single-strands melting enthalpy and is relatively broad compared to the global melting event (about 30 vs 15 °C for the full width at half maxima). Electric birefringence decay measurements show that the phased 45 bp duplex has a rotational time constant of 100 ns at 5 °C which increases to 220 ns above 40 °C. Simple modeling of the dynamics within the junction model for bending yields that the bend per A-tract is 42° at 5 °C, decreasing to 0° above 40 °C. We suggest that this sequence-dependent structure which "melts" at physiological temperatures may be relevant to DNA topology and function.

Although DNA is in principle a rather simple polymer, it is now clear that even at physiological salt and water concentrations there are important sequence-dependent modulations of the classic double B-helical structure of the polymer (Wells & Harvey, 1988). We believe it is very important in molecular biology to understand this sequence-dependent modulation of DNA structure. One of the primary goals in molecular biology is to obtain a detailed, quantitative, and molecular understanding of the manner in which proteins recognize and interact in a base-pair specific manner with the double helix.

It now seems clear that base-pair sequence not only codes for the protein that is to be expressed but also contains vital control information. The manner in which this sequence-dependent information is coded remains a major puzzle. We seek not a cataloging of the sequences that lead to control but an understanding of the physical basis behind the chosen sequences. At present, this information must be gathered by empirical means since we have little predictive power concerning the relationship between sequence and the physical nature of the duplex.

For example, Cocho et al. (1990) have noted a correlation between the base-pair composition and the evolutionary position of the organism from which the DNA was extracted. Further, Cocho has observed that the correlation can be systematized in terms of the strength of the base-pair stacking interaction (Breslauer et al., 1986). In the same vein, there has been a recent flurry of analysis of base-pair sequence autocorrelations as a function of distance along the polymer (Voss, 1992; Peng et al., 1992). These correlations go out to millions of base-pairs, and it is tempting to conclude that long length scale modulation of DNA topology and rigidity might be key to understanding these correlations.

It is our purpose here to use quantitative and physical methods to explore how DNA sequence can control DNA conformation. One specific example has been chosen, which may encourage a broader understanding of how the primary structure of DNA can encode information other than amino acid sequence.

We consider in this paper the altered low-temperature structure of DNA oligonucleotides containing phased $(dA)_n$ tracts. It has been postulated for several years that phased A-tracts in DNA apparently can give rise to "bent" DNA B-helices (Crothers et al., 1990). We explored in a previous paper the unusual, temperature-dependent CD spectrum of the homopolymer dA·dT, the occurrence of the same unusual structure in A-tracts embedded in pseudorandom sequences of "normal" DNA, and the apparent structural consequences of these phased A-tracts in kinetoplast DNA fragments using physical techniques (Chan et al., 1990). We showed that the unusual physical properties of the kDNA fragment, namely, the apparent static bend in the helix backbone, were related to the observation of an unusual structural conformation of the fractionated fragments of homo(dA·dT) but that these anomalies in the structure "melted out" at a temperature *well below* the melting point of the duplex, indicating that the unusual structure giving rise to bent DNA had its origin in

† This work was supported by NIH Grants GM 23509, GM 34469, and CA 47795 (K.J.B. and S.S.C.), NSF Grant 8816340 and ONR Grant N00014-91-J-4084 (R.H.A.), and NIH Grant CA 39527 (M.E.H.).

* Author to whom correspondence should be addressed.

® Abstract published in *Advance ACS Abstracts*, October 15, 1993.

0006-2960/93/0432-11776$04.00/0

a thermodynamically distinct state from the normal B-type duplex and that bent DNA is *not* due to simple, temperature-independent stereochemistry of how base-pairs stack upon each other.

At the time of those experiments we were not able to make any thermodynamic measurements on this premelting transition because direct thermodynamic techniques such as differential scanning calorimetry (DSC) require much larger quantities of high-quality DNA of a uniform known length than what were available. In the absence of direct thermodynamic data it was difficult to know the true origin of the low-temperature anomalies. For example, one possibility is that the bend is due to the increase in the root-mean-square extent of an anisotropically flexible helix (Zhurkin et al., 1991). If the opening angle is viewed as a degree of freedom, one would not expect that the specific heat of the system would exhibit peaks as a function of temperature if the RMS opening angles simply increase with temperature. The other possibility is that the A-tract has a unique structure at low-temperature which changes over some temperature range to normal B-helix parameters. A structural change will result in a change in the degrees of freedom of the system and a corresponding change in the system heat capacity. Further, when two distinct phases meet at a boundary, the strain induced between the two phases could lead to a bending of the helix if the strain is phased with the helix repeat. In fact, such a phenomenon is commonly seen in martensitic phase transitions seen in metal alloys (Perkins, 1975). This bend induced by a discontinuity between dissimilar crystal structures is called the "junction model" (Selsing et al., 1979). The distinction between these two possibilities is quite important, since most theories of bending that have been advanced, either by discontinuities in junctions (Wu & Crothers, 1984), wedges in the base-pair stacking (Bolshoy et al., 1991), or a combination of crystallographic and thermal factors (Olson et al., 1988, 1993), are basically single-phase models which, although they include both sequence dependence to the DNA structure and thermal fluctuations, *do not* consider the possibility of a temperature-dependent phase change in the internal structure of the DNA. If indeed alternate structures are energetically close, then they should be considered when attempts are made to model the way in which DNA can interact with a protein, since under appropriate strain conditions the unstable state can become the stable state thermodynamically.

In order to probe the way that sequence influences structure, it is important to be able to construct sequence isomers containing the same amounts of AT and GC base-pairs but with variable ordering of the base-pairs. In our case, we believe that A-tracts at low temperatures have an unusual structure. The work described in this paper uses synthetic oligo sequences of 45 base pair length in order to systematically explore the unusual behavior of the $(dA{\cdot}dT)_n$ sequence. We choose sequences of 45 bp length because they are long enough to have polymer behavior and to be used in physical techniques such as electric birefringence yet short enough to be produced in sufficient quantities for thermodynamic technique, DSC. The sequence design with phased $(dA)_5$ segments mimics kinetoplast DNA fragments which have $(dA)_n$ tracks ($4 \leq n \leq 6$) repeating almost every 10 base pairs of a length segment over 200 bp. Our synthetic 45-mer duplex has 4 segments of phased $(dA)_5$ tracks separated by five segments of five randomized G·C pairs as shown in the following sequences:

top: 5′-GGCCGAAAAACCGCGAAAAACGGCGAAAAACGCGGAAAAACGCCC

bottom: CCGGCTTTTTGGCGCTTTTTGCCGCTTTTTGCGCCTTTTTGCGGG-5′

As a control, we also designed an isomeric 45-mer duplex with the same base-pair composition but randomized sequences:

top: 5′-GGACAGACACAGACAGAGACACAGCAGACGAGACACAGACACACG

bottom: CCTGTCTGTGTCTGTCTCTGTGTCGTCTGCTCTGTGTCTGTGTGC-5′

These two sets of sequence designs readily promote duplex formation and minimize any single-strand self-association. Further, since the persistence length of random sequence DNA is on the order of 200 base pairs (680 Å), these fragments can be considered as stiff rods in our birefringence measurements. However, since these 45 bp long fragments are synthetically produced, it is quite easy to prepare exactly known sequences which can be compared to theoretical predictions.

EXPERIMENTAL PROCEDURES

Single-Strand DNA Synthesis and Purification. Oligodeoxyribonucleotides were synthesized by the standard β-cyanoethylphosphoramidite method using a Milligen 7500 synthesizer and purified by reversed-phase HPLC (Fritz et al., 1978). The sequences of the oligonucleotides were confirmed by the method of Maxam and Gilbert (1980). The yield of each strand was about 2–4 mg.

Preparation of Duplexes. Since the sequences are not self-complementary, accurate preparation of duplexes with no excess single strands requires accurate knowledge of the number of moles of top or bottom strand before mixing. The most accurate way to determine concentration and hence moles of materials is by UV absorbance, but since the UV absorbance is a function of both the bases and the nearest neighbors (Cantor & Warshaw, 1970), the extinction coefficient must be calculated for a given sequence. The molecular masses of the two top strands are 1.47×10^4 g/mol while the two bottom complementary strands are 1.45×10^4 g/mol. The 45-base strand absorption extinction coefficients at 260 nm in $(mM{\cdot}cm)^{-1}$ were determined theoretically by evaluating the simple sum of the bases and adding in the spectral perturbations by nearest-neighbor interactions. We performed a check on the predicted extinction coefficients by phosphate analysis of each strand, with an accuracy of about ±5%. The theoretical (measured) extinction coefficients were determined to be as follows: phased A strand, 455.9 (438); phased T strand, 382.4 (399); random A strand, 470.4 (450); and random T strand, 387.1 (390). Given the experimental errors, these two sets of values are essentially identical and give confidence in our ability using UV absorbance to do accurate mixing of equal-molar single strands.

Each purified strand was first dissolved in distilled water to give 1–2 mM single strands. We then diluted each strand in 2 mL of a DSC buffer: 10 mM phosphate (P_i), 0.1 M NaCl, and 10 μM EDTA, pH 7.5, to give roughly 120–140 μM concentration. The duplex formation was first optically monitored while titrating one strand with its complement, each at 1 μM. After a minimal optical absorbance had been reached, the titrated solution was transferred to a sealed tube, heated to 95 °C in a large water bath, and annealed slowly by letting the bath cool down to ambient temperature over a period of several hours. The absorbance was remeasured, and the extinction coefficient was calculated for each duplex molarity: phased, 696 $(mM{\cdot}cm^{-1})$; random, 706 $(mM{\cdot}cm^{-1})$. The resulting material migrated as a single band as assessed by gel electrophoresis (10% polyacrylamide in 1 × TBE).

Duplexes were then prepared at high concentrations. For scanning calorimetry, the duplex concentration was set to be in the range of 60–70 μM corresponding to an actual absorption

OD of 42–52 in 1-cm optical path. All duplexes were heat-annealed the same way as described above.

For UV melting experiments and circular dichroism (CD) melting experiments, an appropriate amount from the stock was diluted using the same phosphate buffer to give a final concentration of the order of 1 OD in 1–1.5 mL. For differential scanning calorimetry, each sample at this stock concentration was degassed for about 15 min prior to loading into the sample compartment. The volume needed for a DSC experiment is about 1.5 mL, which means the total duplex weight was about 3 mg.

Circular Dichroism. The CD measurements were recorded on a single-beam spectropolarimeter (Aviv Associates, Model 60DS) equipped with a Peltier temperature controller. On spectral scanning mode, each spectrum, taken at every 5 °C step, was an average of three scans with the subtraction of the buffer spectrum taken at the same temperature as the sample from 350 to 210 nm. On CD melting mode, three or four different wavelengths were selected simultaneously to record temperature scan from 5 to 95 °C by 0.5 °C increment step. After equilibration of each new temperature, each CD point was an average over a 20- or 30-s period with a spectral bandwidth of 2 nm. The selected wavelengths were 350, 270, 250, and 220 nm, which monitored the minimal and the maximal changes of the CD signals over the entire temperature span. We have examined both diluted concentration using 1-cm optical path cuvette and concentrated stock duplex using 0.035-cm optical path cuvette to monitor the CD changes as a function of temperature.

Sample Preparation for Electric Birefringence. The amplitude and hence the signal/noise of the induced birefringence is sensitive to the length of the oriented molecule and the ionic strength of the solution. In general, one wants to use as low a salt concentration as possible. This is particularly important for a relatively small linear molecule, since the amount of orientation decreases with the shorter length of the molecule. However, using too low a salt concentration, below 1 mM, can result in destabilization of the short duplex and lowering of the duplex melting transition temperature. We found that the buffer (EBD buffer) of 1 mM Tris, 4 mM NaCl, and 10 μM EDTA, pH 7.5, gave sufficient signal/noise at 3 kV/cm and maintained reasonably normal melting temperatures (50–60 °C).

A small amount of each duplex from the annealed stock solution was exchanged into this buffer three times and concentrated to about 5 OD/cm using Amicon's Centricon-10. The volume requirement for EBD buffer was only about 50 μL for each run with an optical path of 0.8 cm. Details of the apparatus are given in Chan et al. (1990). In these experiments the pulse generator (Cober 605P) was set to give 2.0-μs pulses at 3 kV/cm at a repetition rate rate of 2 Hz. The pulse width was set so that the birefringence signal had risen to its equilibrium value at the applied electric field. The water-jacketed sample temperature was controlled by a Neslab recirculating water bath, and the actual sample temperature was monitored by a thermocouple embedded in the sample holder wall. The total birefringence signal, from prepulse baseline to postpulse baseline, was averaged on a LeCroy 9200A digital oscilloscope and transferred to a computer for subsequent analysis. The $t = 0$ point was determined with a precision of 10 ns as the point at which the pulse amplitude was returned to zero volts.

UV Absorbance. Temperature-programmed UV melting experiments were done at 260 nm using a Perkin-Elmer spectrophotometer, Model 575, to determine the melting

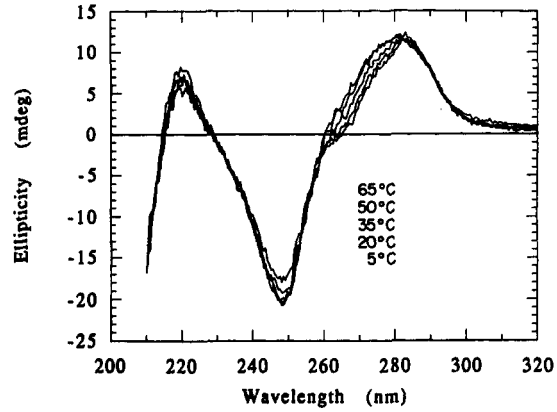

FIGURE 1: Overlay of CD spectra of phased 45 bp at selected temperatures. The temperatures follow the order in which the CD ellipticity decreases at 270 nm from high temperatures (65 °C) to low temperatures (5 °C).

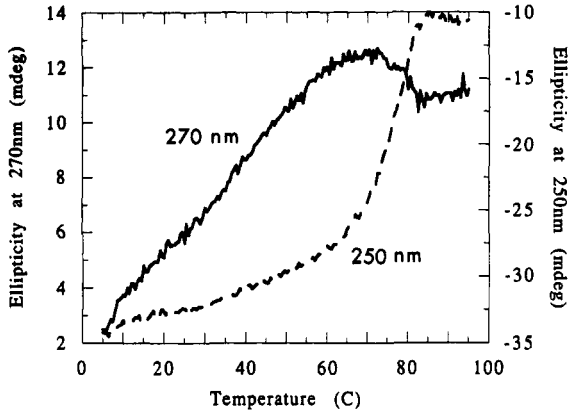

FIGURE 2: CD melting curves at 270 nm (solid line) and 250 nm (dashed line) of the phased 45 bp fragments. These are differential values, with the zero point taken as the CD ellipticity at 0 °C.

temperatures of the duplexes in different buffer conditions before conducting any of the experiments for premelting studies. In DSC buffer, T_m was about 75 °C for phased 45 bp and 70 °C for random duplex. In EBD buffer, the phased duplex melts at about 55 °C while the random duplex melts at about 50 °C. In both instances, the measured T_m's of the optical hyperchromicity were in good agreement with values predicted for fragments with these base compositions.

RESULTS

CD Measurements. We followed the CD spectral change of both phased 45 bp and random 45 bp between 210 and 350 nm every 5 °C between 5 and 80 °C. Figure 1 shows the overlays of the spectral changes for some selected temperatures. The general features of the phased 45 bp CD changes, including the three isoelliptic points, closely resemble those we reported earlier for the kDNA fragments (Chan et al., 1990) while the random 45 bp shows very little change before duplex melting (data not shown). The absolute CD changes we observe for the phased 45 bp duplex are not as pronounced as we found with poly(dA)·poly(dT) fragments. This difference is expected due to the smaller fraction of AT bases in the 45 bp duplex. Figure 2 presents CD melting curves for the phased 45 bp duplex at 270 and 250 nm. The temperature-dependent changes at 270 nm suggest that a conformational transition occurs below 65 °C, before the phased 45 bp duplex globally melts to single strands at about 75 °C, as revealed by the 250-nm melting curve. By contrast, the random 45 bp duplex exhibits CD changes expected for B-type helix: no changes

at 270 nm from 5 to 60 °C and a melting transition at 70 °C observed at 250 nm (data not shown). The premelt transition observed in the phased DNA is independent of concentration of the polymer, as shown by comparison of the profiles of two concentrations differing by a factor of about 30 (data not shown). Since the transition temperature is concentration independent, the conformational transition most likely is intramolecular, although we cannot rule out pseudomonomolecular processes where propagation dominates initiation.

On the basis of the isoelliptic points and the concentration independent melting behavior, we propose that the premelting event corresponds to a single, monomolecular (intramolecular) transition between *two discrete states within the double helix*. This interpretation is to be distinguished from a thermal equilibration between many possible conformations. Assuming a simple two-state monomolecular premelting event in the phased 45 bp duplex, we can subject the data to a van't Hoff analysis as previously described (Marky & Breslauer, 1987) to the phased 45 bp sequence in order to obtain the enthalpy change between the two states. As with the corresponding analyses of the poly(dA)·poly(dT) and kDNA data (Chan et al., 1990), it is very difficult to assign baselines above and below the premelt transition since the CD signal changes continuously from 5 to 60 °C. We have assumed, on the basis of the birefringence decay curves described later, that the bent state is completely occupied below 5 °C and that the normal (linear) state is completely occupied at about 60 °C. With this assumption, we can assign baselines and then calculate from the data in Figure 2 the quantity α, the ratio of the low-temperature state to the high-temperature state. The analysis allows us to convert the experimental ellipticity versus temperature (T) profile into a derived α versus T curve where α corresponds to the fraction in the initial low-temperature state.

The van't Hoff relationship allows one to estimate the enthalpy difference between the two states based upon the temperature dependence of α. The physics of solid-state structural transitions is not well understood, and it is not possible to simply fit the $\alpha(T)$ vs T curve to a model-independent enthalpy. Instead, one measures the slope $d\alpha/dT$ at the midpoint, T_{pm}, of the intramolecular transition where $\alpha = 0.5$, i.e., equal populations of the two states (Marky & Breslauer, 1987). From this value, the van't Hoff enthalpy for the premelting transition, ΔH^{pm}_{vH}, can be calculated using

$$\Delta H^{pm}_{vH} = 4RT_{pm}[d\alpha/dT]_{T_{pm}} \quad (1)$$

where T is the temperature in Kelvin. This value for the enthalpy, ΔH^{pm}_{vH}, corresponds to the effective enthalpic release per cooperative length. On the basis of the assumption that $\alpha = 1$ at 0 °C and $\alpha = 0$ at 65 °C, we find the midpoint of the premelting transition temperature to be 32 ± 2 °C. Using eq 1, we calculated the van't Hoff enthalpy to be 16 kcal/mol per cooperative unit, as compared to the values of van't Hoff enthalpies of 20 kcal/mol reported for poly(dA)·poly(dT) by Herrera and Chaires (1989) and for fragments of kDNA and poly(dA)·poly(dT) by us previously (Chan et al., 1990). Note that the value of the cooperative unit is yet to be determined and is highly model dependent. Despite the assumption noted above, the agreement between the ΔH^{pm}_{vH} for the phased 45 bp duplex reported here with previous determinations suggests that the phased tract in the synthetic 45 bp duplex behaves as the A-tracts in other duplex contexts.

The van't Hoff analysis is based upon two assumptions: (1) The baseline assignments for the high- and low-temperature species are correct; (2) the CD signal measures an order parameter which is related to the fraction of molecules in two states: bent (A-tract) and straight (B-helix) in this case. Although the isoelliptic points are consistent with only two states, bent and straight, there is no guarantee that the CD signal is linearly proportional to the fraction of the bent and straight states. A more direct determination of the premelting transition enthalpy can be obtained calorimetrically, as described in the next section.

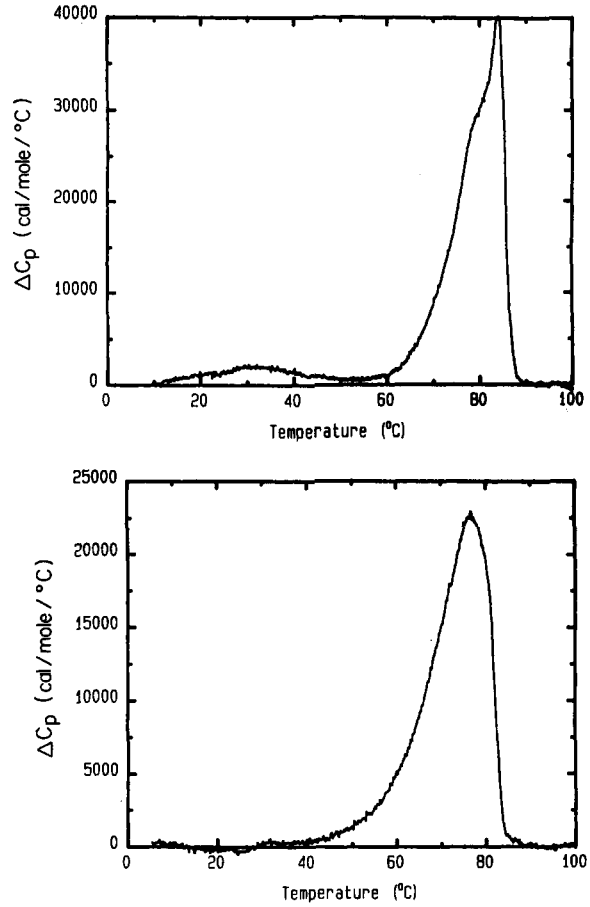

FIGURE 3: Heat capacity, C_p, vs temperature, T, of (a, top) phased 45 bp and (b, bottom) random 45 bp. Since these are raw data, the C_p is in cal/(deg·mol of duplex).

Thermodynamic Evidence for A-Tract Structure Transitions from DSC. Differential scanning calorimetry (DSC) provides a direct measure of the heat released in a thermally induced reaction, although it is still necessary to define baselines and to know accurately the concentration and the volume of the measured material in order to calculate the transition enthalpy.

We have measured the heat capacity changes as a function of temperature for both phased 45 bp and random 45 bp duplexes by differential scanning calorimetry (Microcal, Model MC-2). The transition enthalpy was obtained by integrating the area under the heat profile after the baseline had been subtracted. The duplex concentrations were 62 μM for phased and 71 μM for random sequence, and the volume of the DSC cell was calibrated to be 1.188 mL. Figure 3a shows the calorimetric profiles for the phased sequence and Figure 3b that for random sequence. The large peaks centered around 80 °C (T_m) are from the global duplex melting to the single strands.

Note that the large global melting peak for the phased 45 bp duplex is asymmetrical with a shoulder to the left of the maximum, indicating that there were at least two thermally

Table I: Calorimetric Melting Temperatures and Transition Enthalpies of the Random and Phased 45 bp DNA

parameter	units	random	phased	method
T_m	°C	77	84	
ΔH_{pred}	kcal/(mol dup)	301	422	Breslauer et al. (1986)
(global)	kcal/(mol nn)	6.8	9.6	
ΔH_{dsc}	kcal/(mol duplex)	379 ± 8	434 ± 6	peak area
(global)	kcal/(mol nn)	8.6 ± 0.2	9.7 ± 0.2	
T_{pm}	°C	NA	27 ± 2	
ΔH_{dsc}	kcal/(mol dup)	NA	70 ± 10	peak area
(premelt)	kcal/(mol AA_{step})	NA	4.4 ± 0.6	
	kcal/(mol AT_{pair})	NA	3.5 ± 0.5	

resolved events associated with complete duplex melting. We assume that the left shoulder reflects the local strand separation of the phased A·T tracts, and the higher temperature part is due to the strand separation of the random G·C tracts (Breslauer et al., 1986). The profile for the random 45 bp duplex is much more symmetric as expected since there are no extended AT or GC tracts. Thus, even for global strand separation, melting of the AT tracts and the GC tracts of the phased 45 bp retain some degree of autonomy.

The upper half of Table I shows the DSC-derived enthalpy changes of the *global* strand separation of the phased and random sequence 45 bp duplexes. For comparative purposes, the predicted value using nearest-neighbor data also is tabulated (Breslauer et al., 1986). Note that the ΔH_{dsc} of 434 ± 6 kcal/mol of phased 45 bp duplex is very close to the predicted value of ΔH_{pred} of 422 kcal/mol duplex. The corresponding average ΔH_{dsc} per base pair is 9.7 ± 0.2 kcal/mol of nearest neighbor (nn) versus the predicted 9.58 kcal/mol nn. We find this to be excellent agreement between the predicted and observed strand separation enthalpy changes for the phased 45 bp duplex. By contrast, relatively poor agreement between the predicted and observed global transition enthalpies is found for the random duplex. At present, we have no explanation for this disparity.

Significantly, inspection of Figure 3 reveals a *small and broad peak from about 10 to 55 °C for the phased 45 bp duplex that is absent in the random 45 bp duplex.* This peak is separated from the main duplex global melting peak. Further, this peak is not observed when the *in situ* reannealing process is performed quickly, that is, if the phased strand separated duplex is cooled within minutes from 100 to 0 °C [possibly due to down-shifting of the registry of the phased $(dA)_5$ tracks]. However, the transition can be brought back by a reannealing process using a manually controlled stepwise process over a period of 2 or more hours, moving particularly slowly about the T_m range. When one cycles the temperature between 5 and 60 °C without allowing the duplex to melt, the premelting ΔH persists even with fast cooling back down to 5 °C. Thus, as long as the well-annealed duplex is not disrupted, the premelting transition is detectable calorimetrically.

From integration of the area under the premelting curve, we calculate that $\Delta H_{dsc}^{pm} = 70 \pm 10$ kcal/mol of duplex. This value corresponds to only about 16% of the total enthalpy change for the global melting of the duplex to single strands. The full width at half maxima is about 30 °C, relatively broad compared to global melting peak (about 15 °C). Since the random sequence isomeric 45 bp presents no evidence of a premelting event, it is tempting to assume that the premelt enthalpy change from the phased duplex comes *only* from the dA·dT tracts, with *no* contribution from the dG·dC portions of the duplex. In such a case, the normalization factor to extract the energy per unit undergoing the phase transition should be either 20 bp of A·T or 16 steps of contiguous AA nearest neighbors (nn), which translates into either 3.5 kcal/mol of AT bp or 4.4 kcal/mol of AA nn or step. This value falls very much in the range of a hydrogen bond energy (Freier et al., 1986; Shirley et al., 1992; Remeta et al., 1993). The T_{pm} of the transition is centered at 32 ± 5 °C, in agreement with the CD data. The lower half of Table I summarizes these results.

Field-Free Birefringence Decay. The previous two sections have provided evidence for the fact that there is a premelting structural change and have provided values for the enthalpy change associated with the structural transition. We expect from our previous work with kinetoplast fragments (219 bp) that the phased A-tract fragments will also be *bent* at temperatures below the premelting transition and straight above them (Chan et al., 1990).

At the time, we were able to use both electric birefringence and singlet depletion anisotropy measurements to qualitatively probe the amount of bending in the kDNA fragments. However, a quantitative analysis could not be performed since the fragments were close to a persistence length long. For long fragments, the coupling of internal deformation and helix flexibility is an intractable hydrodynamics problem. However, since the synthetic duplexes studied here are only 45 base-pairs in length, questions of flexibility become less important. We did not attempt to make optical measurements using intercalated dyes on these duplexes since the intercalated dyes could disrupt the structure of these short molecules and provide questionable results. Thus, in this work we have used only field-free birefringence decay as a probe of the curvature of the helix backbone since it can be used on native structures without perturbation.

The experimental apparatus used to make these measurements has been described in several previous publications (Chan et al., 1990; Hong et al., 1992). The main difficulty in these measurements was the short length of the 45 bp duplex: the amount of alignment of the polymer scales roughly exponentially with the length of the polymer fragment (which is presumed to be proportional to the size of the aligning induced electric dipole moment). Since the size of the observed monitoring light intensity change varies with the square of the net polarization rotation, short fragments give very small, fast signals. Adequate sensitivity was achieved only by using DNA concentrations of about 5 OD measured at 260 nm and using a low-salt buffer to minimize shielding of the induced dipole moment. We settled on a Tris-based EBD buffer as described above which was of high enough salt concentration to maintain helix stability and low enough conductivity to allow a reasonable birefringence signal. We have confirmed that the premelting transition of interest is not altered in the EBD buffer system as assessed by CD.

Figure 4 shows the raw (unprocessed) birefringence response of both the phased A-tract fragment and the isomeric random-sequence fragment at 20 °C for approximately 3 kV/cm fields of duration $\mathcal{T}$ equal to 1 μs. It is clear that the two sequences at this temperature have substantially different responses: the random 45 bp duplex is slower to be aligned by the applied field and slower to depolarize in the zero field than the phased 45 bp duplex. The data here will concentrate on the field-free

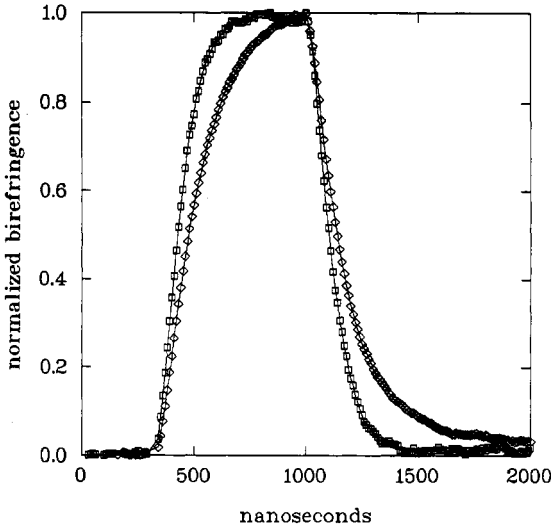

FIGURE 4: Raw birefringence decay curve at 20 °C for 45 bp long containing a random sequence (◇) and four phased $(dA)_5$ tracts (□). A clear difference in the response of the phased and nonphased sequence can be seen, with the phase sequence showing faster field-free decay. The rise time of the system was measured to be under 50 ns by measuring water birefringence.

decay, which is better understood than the field-dependent orientation. We have carried out a series of measurements of the birefringence decay of these two sequences as a function of temperature every 5 °C, up to the melting temperature of the double-helical structure.

We first consider the birefringence decay of a rigid rod of length L and radius b in a medium of viscosity η at temperature T. If we assume that the DNA molecule has two degenerate diffusion constants $D_1 = D_2 = D_\perp$ for rotation about the two short axes (tumbling) and a third diffusion constant $D_3 = D_\parallel$ for rotation about the long axis (spinning), then the field-free decay of a rigid rod consists of three exponentials (Wegener, 1986):

$$a(t) = \sum_{i=1}^{3} C_i(\mathcal{T}) \exp(-\tau_i t) \tag{2}$$

The constants $C_i(\mathcal{T})$ are in general dependent on the duration $\mathcal{T}$ of the aligning pulse and the relative orientation of the polarizability tensor β of rotational diffusion tensor D_r. If the aligning pulse width is set to be wide enough that the equilibrium value of alignment is obtained, then the pulse dependent nature of the C_i can be neglected. Since the relative alignment of the polarizability tensor with the diffusion axis is not known, we treat the C_i as fitting variables.

The three exponential time constants τ_i are given by

$$1/\tau_1 = 2D_\perp + 4D_\parallel \tag{3}$$

$$1/\tau_2 = 5D_\perp + D_\parallel \tag{4}$$

$$1/\tau_3 = 6D_\perp \tag{5}$$

The 45 bp duplexes are approximately 153 Å, much shorter than the approximate persistence length of DNA of 600 Å (Hagerman, 1988). Thus, it is a good approximation to treat these molecules as rigid rods. The diffusional constants can be calculated from the expressions of Broersma (1960) for a right circular cylinder of radius b and length L at temperature T:

$$D_\perp = \frac{3k_BT}{8\pi\eta L^3} \tag{6}$$

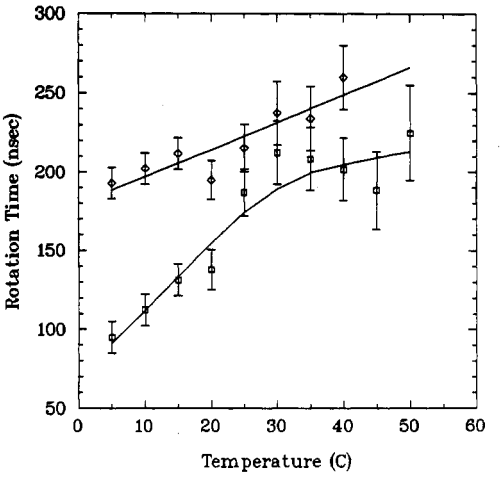

FIGURE 5: Plot of the slowest birefringence decay normalized time constant τ_3 vs temperature for the random 45 bp (◇) and the phased 45 bp (□). As discussed in the text, the time constant τ_3 determined from curve fitting of the data has been renormalized by multiplying with the factor $[\eta(293\text{ K})/\eta(T)] \times [293/T]$. The solid line through unphased (◇) data points is a fit to a linear relationship between the unphased rotation time and temperature, the solid line through the phased (□) data points is simply to guide the eye.

$$D_\parallel = \frac{k_BT}{8\pi\eta b^2 L} \tag{7}$$

where k_B is Boltzmann's constant. We will assume here that the radius b of the cylinder is much smaller than the length L. Since the diffusion constants scale with T/η, we have multiplied the time axis in the plots by the quantity T/η in order to compensate for the known change in the viscosity of water with temperature and the change in the Brownian driving force. For the simplest case,

$$\frac{T\tau_3}{\eta} = \frac{8\pi L^3}{6k_B} \tag{8}$$

Note that the rotational time for end-over-end tumbling is very sensitive to the length of the DNA, that is, goes as the third power of the length. Furthermore, if there is no change in the length of the molecule over any temperature, the quantity, $T\tau_3/\eta$, will have constant value, independent of temperature. Conversely, if the rod is bent into a circle of radius R, hydrodynamics tells us the effective "length" of the object begins to approximate the maximum extension, L/π.

The random-sequence isomer 45 bp should be accurately fit by the above equations for the diffusion constant of a straight rod. Assume an ordering B-form geometry (r = 3.4 Å), the length L of the duplex is 153 Å, and the hydrodynamic radius b is assumed to be 12 Å. We then find that the three time constants (τ's) are 1.8×10^{-8}, 6.0×10^{-8}, and 2.8×10^{-7} s. Since the fall time of our pulse generator is 5×10^{-8} s, the fastest time constant not observable and the second one is highly convoluted with the fall time. Since we are only interested in this work with the longest motions due to the effective length of the molecule, the birefringence decay curves were fit to a two-exponential decay curve. Only the longest decay constant was deemed sufficiently free of electric pulse fall time convolution to be useful.

Figure 5 shows a coplot of the corrected field-free longest decay time constants versus temperature for the random 45 bp (◇) and for the phased 45 bp (□). The corrected rotation time of the random sequence is not totally independent of temperature and shows a small linear increase as shown by the solid line. We do not understand the origin of this effect; it may be due to a linear expansion of the helix with

temperature. The temperature coefficient of expansion of a linear object $\delta(T)$ is defined by $\delta = \Delta L/L\Delta T$, where L is the length of the object at temperature T, and ΔL is the length increase of the object upon being warmed by an amount ΔT. Note that $\Delta L/L = (L_2 - L_1)/L_2 = [1 - (L_1/L_2)]$, and that $L \sim \tau^3$, where τ is the rotation time from the birefringence relaxation. Reading the rotation times from Figure 5, we get $\delta = [1 - (240/190)^{1/3}]/[40° - 5°] = 2.3 \times 10^{-3}$ K^{-1}. This is about three times the value for water at 20 °C.

Unfortunately, we have not found any literature values for the temperature coefficient expansion of DNA, and because of our uncertainty concerning what is happening here, we have elected to use the *average* value for the corrected rotation times of the random sequence duplex (2.1×10^{-7} s, in good agreement with the expected 2.8×10^{-7} s decay time for a 45 bp rod) for the sequent analysis.

The phased-sequence duplex decay times (corrected) show a substantially larger temperature dependence; at low temperatures the rotation times are substantially shorter than the random duplex times but approach the random sequence values at temperatures above 35 °C. Hagerman (1984) also observed decreased molecular tumbling times for phased oligo-A duplexes for 121 bp restriction fragments at 3 °C. However, it is clear that the shortened birefringence decay times occur only at lower temperatures; at temperatures greater than 35 °C the normalized decay times become the same, within experimental error, as the decay times for the random sequence duplex, indicating that the DNA fragment is now straight. It is clear from these data, as was also seen in the kDNA work, that the electronic changes (CD and UV absorbance data), the thermodynamic transition (DSC data), and the rotational dynamics (EBD data) all see the same process.

In order to estimate the radius of curvature of the phased duplex at low temperature, we need to be able to calculate the birefringence decay of a circularly bent rod. The calculation of the diffusion tensor for a centrally bent rod is very difficult, and some approximations must be made. The reader must be aware then that since we are unsure of the origin of the increase in the random sequence rotation times with temperature, there may be substantial errors involved in assuming with the phased DNA that *all* the increase in rotation times is due to straightening of the helix axis. However, in the absence of further information concerning the thermal coefficient expansion of DNA, we present the simplest model possible. The angles we calculate below could be substantially smaller if we could factor in a known temperature coefficient of expansion.

All attempts that we are aware of model the DNA as bent at a particular point along the helix through an angle ψ. Of course, since the structural perturbation seems correlated with A-tracts distributed periodically along the helix, the truth probably is that the total bend occurs as a sum of bends occurring at junctions between the A-tracts and normal DNA B-helix as discussed by Levene et al. (1986).

As a first approximation to the correct form of the decay, we can use the single bend approximation to obtain the end-to-end distance of the bent molecule and from this obtain the bend angle per junction. In principle, the computer dynamics simulations of Mellado and de la Torre (1982) for rigid string of beads bent through an angle ψ ($\psi = 0°$ in our notation corresponds to a straight, unbent rod) should allow us to come up with at least a plausible estimate of the total bend of the molecule. Unfortunately, the analysis was done only for a rod of length/diameter ($L/2b$) of 72, corresponding to a DNA fragment of length 500 base-pairs. Empirically, Mellado and de la Torre believe that the time constant ratios they derive are only weakly dependent on $L/2b$, but there is no physical basis for this surmise, and it is not at all clear that for our $L/2b$ of approximately 6 that the weak dependence is still valid. The reader is thus cautioned to take the following result with a grain of salt. Table 2 from the paper by Mellado and de la Torre (1982) shows that in the case of a rod bent exactly in the middle (in their notation, $\gamma = 1/2$) that a bend angle ψ (χ in their Table 2 is $180° - \psi$) of approximately 100° will give our observed shortening of the longest time constant by a factor of 2. Figure 6a shows a strictly schematic picture of these angles.

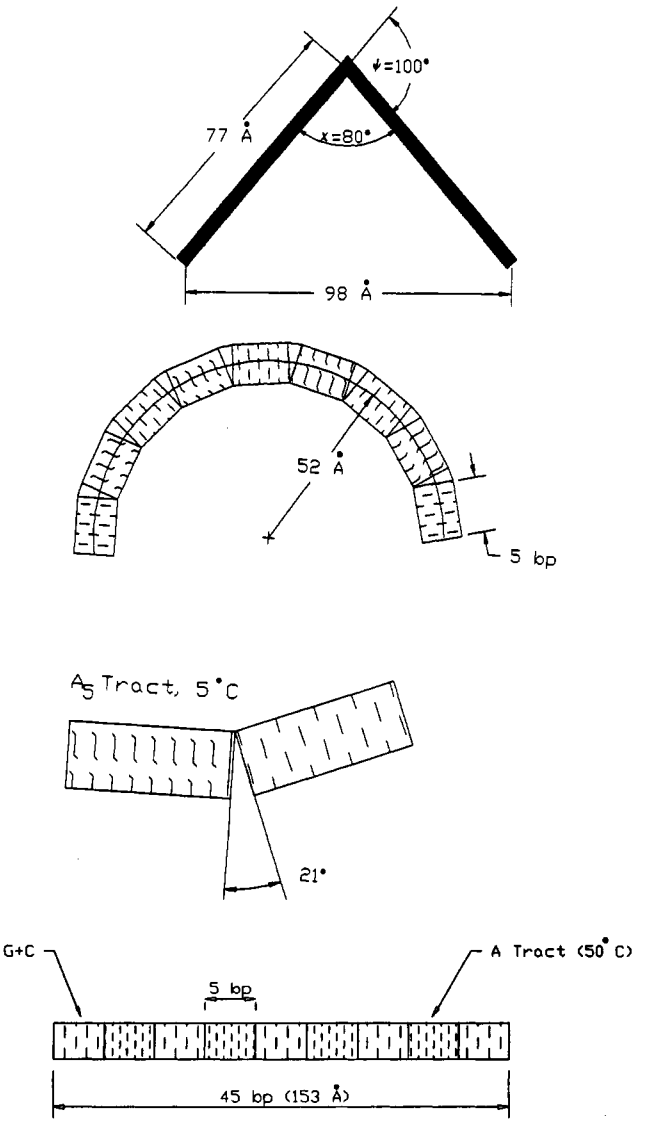

FIGURE 6: Schematic drawing of the phased 45 bp to illustrate the angles and conformations discussed in the text. (a, top) Rod bent at the center with opening angle ψ of 100°. The rod is the same length as a 45 bp long DNA polymer, and the end-to-end distance of the bent rod is 98 Å. This configuration would yield a rotational diffusion rate half the value of the equivalent straight rod. (b, middle) Rod bent by a succession of junctions between A-tracts and normal B-helix regions. This simulation assumes a temperature T of 5 °C. The angle between each successive section is 21°. The net end-to-end distance of 98 Å needed to model our birefringence results is reproduced in this simulation. The insert shows the junction angle of 21° between the A-tract and the G+C tract at 5 °C. (c, bottom) Same rod at a temperature $T = 50$ °C, where the A-tracts have the same structure as B-helix, and the junction bend angle is now 0°.

The end-to-end distance of a 153-Å long rod (45 bp) bent at the midpoint through an angle ψ of 100° is 98 Å (equivalent in 2 × the hydrodynamic radius of gyration to a 29 bp long

straight rod), and a 45 bp rod bent into an arc of radius R = 52 Å will have the same end-to-end distance. Since there are four A-tracts (and hence eight A-tract junctions) in our polymer, we obtain within the junction model that the bend angle at each junction is approximately 21° *at 5 °C*. Figure 6b shows a schematic representation of the angles involved. A junction bend angle of 21° is not in agreement with the value of 9° cited by Crothers et al. (1990), in their excellent minireview. Note that the effective bend angle is a strong function of temperature since the bend disappears above 40 °C. An identical calculation of bending angle derived from the EBD data at 25 °C (Figure 5) generates an angle of approximately 12° per junction. Electrophoresis and physical analyses which have given rise to the "canonical" 9° angle were done at room temperature. A more careful analysis of the hydrodynamics of uniformly curved rods and careful control of gel temperatures while running will perhaps lead to better agreement among the different experiments. If indeed the DNA molecule straightens out with temperature, then the numbers for the bend angle we arrive at here are a substantial *overestimate* of the actual bend angle. Figure 6c shows a schematic of the expected structure of the 45 bp phased duplex at temperatures above 40 °C, where the sequence is now straight.

It is interesting to note that DNA structures based upon crystallographic data and energy refined for our phased 45 bp duplex predict a bend radius R of 109 Å (W.K. Olson and A.R. Srinivasan, personal communication), much larger than our low temperature radius of R of 52 Å. Of course, one of the points of this paper is that computer simulations must also predict an increase in the radius of curvature with temperature, leading to a radius of curvature at 50 °C equal to infinity, that is, a straight rod! It is clear from the works of Olson et al. (1988) and Zhurkin et al. (1990) that there are systematic effects to the angles between base-pairs depending on composition, but we must not forget the instability of the A-tract configuration with increasing temperature.

DISCUSSION

Molecular Aspects of A-Tract Conformation. The previous sections have presented experimental evidence that the phased 45-mer duplex experiences a cooperative phase transition (mild compared to duplex melting transition) that also results in an unusual change in the hydrodynamic radius of the DNA polymer. We stress that the thermodynamic results unequivocally show that there is a true change in state of the phased DNA molecule at the premelting structural transition. Several workers have proposed static structural models for the induced curvature in phased DNA helices that predict a temperature *independent* curvature of the helix. We feel that surely temperature-independent conformation parameters cannot explain the data described here or in our previous communication (Chan et al., 1990). Further, since the state change which we have detected for phased oligo-dA containing duplex occurs near physiological temperatures at physiological ionic strength, its existence may be of biological significance. The thermodynamic results of this work unequivocally call for a state change in the system between bent and straight models, and we suggest that the presence of additional states be considered.

We believe that a possible explanation for our data, similar to that proposed by Klug and his colleagues (Nelson et al., 1987), is that, in a sequence with a track of three or more dA, a three-centered hydrogen bond can form cross-strand from adenine diagonally to the next thymine, deform the A·T base-pair coplanar conformation, and stabilize the propeller twist between the A·T pair as observed by X-ray crystallographers (Nelson et al., 1987; Coll et al., 1987; Yoon et al., 1988). The most direct identification of the two states would be the presence of a three-center hydrogen bond at low temperatures and a standard two-center hydrogen bond at higher temperatures. We must note, however, that our proposed bend between the junction of the $(dA)_5$ tracts and randomized GC tracts 21° at 5 °C is not in accord with the crystallographic data, once again stressing that solution conformation of DNA may be quite different from crystal structures.

Conclusions. This paper uses calorimetric, optical, and birefringence methods to show that, under physiological conditions, oligo-A tracts in duplex DNA can undergo an internal structural transition. The midpoint of this structural transition occurs near 30 °C and has an enthalpy change of either 3.5 kcal/mol AT pair or 4.4 kcal/mol AA step. Either quantity is approximately what is expected from the breakage of a single hydrogen bond. An equivalent conclusion is drawn from both optical data (CD) and calorimetric analysis. A crucial aspect of this transition is that it is well modeled as a two-state structural transition between a low-temperature oligo-A conformational state which is a variant of the B-form duplex and a high-temperature conformer which appears to assume a duplex formation which is more similar to the canonical B form. Using EBD method, we have shown that this temperature-dependent transition is accompanied by straightening of the duplex.

One possible way to interpret these observations is with the junction model, although we hasten to add in no way do we prove the model. In the junction model, bending results from the interface between phased oligo-A elements and random sequence elements: at low temperature, a structural bend forms at the interphase between the oligo-A tract and random sequence section because the secondary structure of the oligo-A tract is atypical. At high temperature, where the secondary structure of an oligo-A segment becomes similar to that of random sequence DNA, the junction disappears and the helix straightens. On the basis of EBD data in the low-temperature range, we calculate a radius of curvature of about 52 Å for the phased 45 bp DNA duplex in this study. In the context of a junction model, this corresponds to approximately 21° of bending per junction formed at the ends of the low-temperature oligo-A conformer. Above 30 °C, this bending angle gradually goes to zero. We find it hard to see how the wedge model, which relies upon temperature-independent crystallographically derived angular displacements, can explain the strong temperature effects observed here.

ACKNOWLEDGMENT

We thank Prof. Wilma K. Olson and Dr. A. R. Srinivasan for valuable discussions and for sharing the results of their simulations. We also thank the anonymous referees for suggesting substantial improvements to the text.

REFERENCES

Bolshoy, A., McNamara, P., Harrington, R. E., & Trifonov, E. N. (1991) *Proc. Natl. Acad. Sci. U.S.A. 88*, 2312–2316.

Breslauer, K. J., Frank, R., Blocker, H., & Marky, L. A. (1986) *Proc. Natl. Acad. Sci. U.S.A. 83*, 3746–3750.

Broersma, S. (1960) *J. Chem. Phys. 32*, 1626–1631.

Cantor, C. R., Warshaw, M. M., & Shapiro, H. (1970) *Biopolymers 9*, 1059–1077.

Chan, S. S., Breslauer, K. J., Hogan, M. E., Kessler, D. J., Austin, R. H., Ojemann, J., Passner, J. M., & Wiles, N. C. (1990) *Biochemistry 29*, 6161–6171.

Cocho, G., Rius, J. L., Miramontes, P., & Medrano, L. (1990) in *Quasycristals and Incommersurate Structures* (Yacaman, M. J., Romeu, D., Castano, V., & Gomez, A., Eds.) pp 465–475, World Scientific, Teaneck, NJ.

Coll, M., Frederick, C. A., Wang, A. H.-J., & Rich, A. (1987) *Proc. Natl. Acad. Sci. U.S.A. 84*, 8385–8389.

Crothers, D. M., Haran, T. E., & Nadeau, J. G. (1990) *J. Biol. Chem. 265*, 7093–7096.

Freier, S. M., Sugimoto, N., Sinclair, A., Alkema, D., Neilson, T., Kierzek, R., Caruthers, M. H., & Turner, D. H. (1986) *Biochemistry 25*, 3214–3219.

Fritz, H.-J., Belagaje, R., Brown, L. E., Fritz, R. H., Jones, R. A., Lees, R. G., & Khorana, H. G. (1978) *Biochemistry 17*, 1257–1267.

Hagerman, P. J. (1984) *Proc. Natl. Acad. Sci. U.S.A. 81*, 4632–4636.

Hagerman, P. J. (1988) *Annu. Rev. Biophys. Biophys. Chem. 17*, 265–286.

Herrera, J. E., & Chaires, J. B. (1989) *Biochemistry 28*, 1993–2000.

Hong, M. K., Narayan, O., Goldstein, R. E., Shyamsunder, E., Austin, R. H., Fisher, D. S., & Hogan, M. E. (1992) *Phys. Rev. Lett. 68*, 1430–1433.

Levene, S. D., Wu, H.-M., & Crothers, D. M. (1986) *Biochemistry 25*, 3988–3995.

Marky, L. A., & Breslauer, K. J. (1987) *Biopolymers 26*, 1601–1620.

Maxam, A., & Gilbert W. (1980) *Methods Enzymol. 65*, 499–560.

Mellado, P., & de la Torre, J. G. (1982) *Biopolymers 21*, 1857–1871.

Nelson, H. C. M., Finch, J. T., Luisi, B. F., & Klug, A. (1987) *Nature 330*, 221–226.

Olson, W. K., Marky, N. L., Jernigan, R. L., & Zhurkin, V. B. (1993) *J. Mol. Biol. 232*, 530–554.

Olson, W. K., Srinivasan, A. R., Hao, M., & Nauss, J. L. (1988) *Struct. Express. 3*, 225–242.

Peng, C.-K., Buldyrev, S. V., Goldberg, A. L., Havlin, S., Sciortino, F., Simons, M., & H. E. Stanley (1992) *Nature 356*, 168–170.

Perkins, J. (1975) *Shape Memory Effects in Alloys*, Plenum Press, New York.

Remeta, D. P., Mudd, C. P., Berger, R. L., & Breslauer, K. J. (1993) *Biochemistry 32*, 5064–5073.

Selsing, E., Wells, R. D., Alden, C. J., & Arnott, S. (1979) *J. Biol. Chem. 254*, 5417–5422.

Shirley, B. A., Stannssens, P., Hahn, U., & Pace, C. N. (1992) *Biochemistry 31*, 725–732.

Voss, R. (1992) *Phys. Rev. Lett. 68*, 3805–3808.

Wegener, W. A. (1986) *J. Chem. Phys. 84*, 5989–6004.

Wells, R. D., & Harvey, S. C., Eds. (1988) *Unusual DNA Structures*, Springer Verlag, New York.

Wu, H.-M., & Crothers, D. M. (1984) *Nature 308*, 509–513.

Yoon, C., Prive, G. G., Goodsell, D. S., & Dickerson, R. E. (1988) *Proc. Natl. Acad. Sci. U.S.A. 85*, 6332–6336.

Zhurkin, V. B., Gorin, A. A., Charakhchyan, A. A., & Ulyanov, N. B. (1990) in *Theoretical Biochemistry and Molecular Biophysics* (Beveridge, D. L., & Lavery, R., Eds.) pp 409–429, Adenine Press, Guilderland, NY.